



# Optimized Automated Data Analysis for the Cytokinesis-Block Micronucleus Assay Using Imaging Flow Cytometry for High Throughput Radiation Biodosimetry

M. A. Rodrigues,<sup>1,2</sup> C. E. Probst,<sup>1</sup> L. A. Beaton-Green,<sup>2</sup> R. C. Wilkins<sup>2\*</sup>

<sup>1</sup>Amnis - MilliporeSigma, Seattle, WA, 98119

<sup>2</sup>Environmental and Radiation Health Sciences Directorate, Health Canada, Ottawa, Ontario, Canada

Received 12 November 2015; Revised 5 May 2016; Accepted 10 May 2016

Additional Supporting Information may be found in the online version of this article.

\*Correspondence to: R. C. Wilkins; Consumer and Clinical Radiation Protection Bureau, Health Canada, 775 Brookfield Road, Ottawa, Ontario, Canada. E-mail: Ruth.Wilkins@hc-sc.gc.ca

Published online 6 June 2016 in Wiley Online Library (wileyonlinelibrary.com)

DOI: 10.1002/cyto.a.22887

© 2016 The Authors. Cytometry Part A published by Wiley Periodicals, Inc. on behalf of ISAC

This is an open access article under the terms of the Creative Commons Attribution-NonCommercial License, which permits use, distribution and reproduction in any medium, provided the original work is properly cited and is not used for commercial purposes.

## • Abstract

The cytokinesis-block micronucleus (CBMN) assay is a well-established technique that can be employed in triage radiation biodosimetry to estimate whole body doses of radiation to potentially exposed individuals through quantitation of the frequency of micronuclei (MN) in binucleated lymphocyte cells (BNCs). The assay has been partially automated using traditional microscope-based methods and most recently has been modified for application on the ImageStream<sup>X</sup> (IS<sup>X</sup>) imaging flow cytometer. This modification has allowed for a similar number of BNCs to be automatically scored as compared to traditional microscopy in a much shorter time period. However, the MN frequency measured was much lower than both manual and automated slide-based methods of performing the assay. This work describes the optimized analysis template which implements newly developed functions in the IDEAS<sup>®</sup> data analysis software for the IS<sup>X</sup> that enhances specificity for BNCs and increases the frequency of scored MN. A new dose response calibration curve is presented in which the average rate of MN per BNC is of similar magnitude to those presented in the literature using automated CBMN slide scoring methods. In addition, dose estimates were generated for nine irradiated, blinded samples and were found to be within  $\pm 0.5$  Gy of the delivered dose. Results demonstrate that the improved identification accuracy for MN and BNCs in the IS<sup>X</sup>-based version of the CBMN assay will translate to increased accuracy when estimating unknown radiation doses received by exposed individuals following large-scale radiological or nuclear emergencies. © 2016 The Authors. Cytometry Part A published by Wiley Periodicals, Inc. on behalf of ISAC

## • Key terms

cytokinesis-block micronucleus assay; automated MN analysis; imaging flow cytometry; biodosimetry; population triage; ImageStream<sup>X</sup>

## INTRODUCTION

It is desirable to estimate doses received by individuals potentially exposed to ionizing radiation following a radiation accident as quickly as possible. When physical dosimetry through the use of dosimeters is not possible, such as in the case of a large-scale radiological emergency, biological dosimetry must be used to determine the dose. Rapid and accurate dose estimations are necessary to determine the proper treatment course for individuals requiring medical attention as well as to provide reassurance to those who have not been exposed. Based on the current capabilities of biodosimetry methods, it has been suggested that individuals receiving whole body doses of less than about 1.5–2 Gy can be followed as outpatients, but those receiving significant doses (>2 Gy) should receive medical treatment in hospital (1,2). The median lethal dose (LD<sub>50</sub>) for total body doses of ionizing radiation in humans is generally accepted to be 4 Gy (3). Above the 4 Gy threshold, clinical symptoms such

as high fever, infection and bleeding will manifest themselves within a few days of exposure and medical treatment is likely to begin before dose estimates from biodosimetry are available. However, below this threshold these physical symptoms may not appear for several weeks and as such, rapid and accurate dose estimations for individuals exposed to doses below the LD<sub>50</sub> is essential.

The cytokinesis-block micronucleus (CBMN) assay is frequently used in radiation biodosimetry to estimate unknown doses by correlating the rate of micronuclei (MN) per binucleated cell (BNC) in peripheral blood lymphocytes to a dose (4,5). The assay is traditionally performed using manual microscopy and is capable of generating accurate and reproducible dose estimations between 0.3 and 4 Gy (6–8). A number of studies have illustrated that linear-quadratic dose response calibration curves can be obtained using automated or semi-automated slide scoring with the MNScore software module on the Metafer slide scanning platform (MetaSystems, Germany) (7–10). The results of these works indicated that the overall MN frequency in these curves was reduced at higher doses (3 or 4 Gy) by a factor between one and a half and three when compared to manual slide scoring. The reduced number of MN in automated slide scoring appears to be related to the strictness of scoring criteria in image analysis that can cause MN that would be typically scored manually to be missed. For example, MN that are in very close proximity to the main nucleus may be missed by automated systems (8,10). This is a limitation to the sensitivity of the assay and its applicability in the low dose region; however, it is less of an issue for rapid dose estimation in the higher dose regions.

A traditional flow cytometry based version of the MN assay in the field of toxicology has been previously described (11) and over the last several years has been configured into a commercially available kit by Litron Laboratories (12–15) that can be performed on a number of cell lines including mouse lymphoma and TK6 cells. In this method, MN are liberated through lysis of the cell membrane and scored through application of a data analysis template that differentiates MN from the main nuclei. The increase in the number of MN can be directly correlated to the toxicity of various compounds and the method has had considerable success in the field of toxicology. One of the limitations of this assay, however, is the generation of false positives by apoptosis inducing compounds that are not necessarily genotoxic (14) thus requiring validation by manual microscopy. Furthermore, this method is not directly applicable to radiation biodosimetry. In the CBMN assay for radiation biodosimetry, the fundamental parameter of measure is the rate of MN per BNC in human lymphocyte cells in first mitosis (16). To quantify this parameter, MN must be scored inside the cytoplasm of a BNC and therefore, the Litron Laboratories method is less than ideal.

A novel method recently developed by our group (17–19) uses imaging flow cytometry (FCM) on the ImageStream<sup>X</sup> (IS<sup>X</sup>) imaging flow cytometer (MilliporeSigma, Billerica, MA) to automate the CBMN assay. The IS<sup>X</sup> system combines the speed of traditional FCM with the high resolution image capabilities of microscopy. Similar to traditional FCM, cells are

labelled with fluorescent dyes and are passed in suspension through the flow cell of the cytometer. In the IS<sup>X</sup>, a bright-field (BF) LED light source and at least one solid state laser (405, 488, and 658 nm in our system) orthogonally interrogate each cell, creating transmitted and scattered light signals. The transmitted and scattered light is collected by one of three high numerical aperture lenses (20×, 40×, or 60×) and undergoes spectral decomposition into specific wavelength ranges within roughly 400–800 nm. The wavelength ranges are then focused onto separate channels of a charge-coupled device (CCD) camera that takes the place of photomultiplier tubes found in traditional flow cytometers. Each channel captures optically divided sub-images which can be viewed individually or can be combined to view the co-location of several signals. In this way, the IS<sup>X</sup> generates high resolution imagery for each cell that passes through the instrument that allows for visual confirmation of micronucleus identification (20–22). This is a substantial advantage over traditional FCM methods.

The IS<sup>X</sup> is capable of capturing high-resolution images of individual cells at a rate of up to 5,000 cells per second. The new IS<sup>X</sup>-CBMN method is able to process cell samples suspended in solution and eliminates the need to create microscope slides, thereby reducing the time required for sample preparation (17–19). All images captured on the IS<sup>X</sup> are saved to a data file which is analyzed using the Image Data Exploration and Analysis Software (IDEAS<sup>®</sup>) built specifically for the IS<sup>X</sup>. Previously, we generated dose response calibration curves from 0–4 Gy (17,19) and 0–10 Gy (18) but in both cases, while a large number of BNCs were scored (about 2,000), a reduction in MN frequency by a factor of about 5–10 was observed when compared to curves generated by automated and manual slide-scoring methods respectively.

This paper describes the optimization of the IDEAS analysis template for identifying and scoring BNCs and MN in the IS<sup>X</sup>-based version of the CBMN assay. In this work, we re-analyzed existing data in order to demonstrate improvements in the accuracy of identifying and separating BNCs from other cells and cellular debris, as well as improved detection of MN through the use of a newly developed MN mask. The resulting increase in MN frequency is evident in the improved dose response calibration curve in which the rate of MN per BNC is comparable in magnitude to those presented by other authors using automated slide-scoring versions of the CBMN assay. Finally the improved accuracy of the template is evidenced by the re-analysis of blinded samples to generate dose estimations to within  $\pm 0.5$  Gy of the delivered dose following only 5 minutes of data collection on the IS<sup>X</sup>.

## MATERIALS AND METHODS

### Blood Collection and Irradiation, the CBMN Assay and Data Collection on the IS<sup>X</sup>

Blood collection, irradiation, and processing was performed previously as described by Rodrigues et al. (17–19) and all data was saved as raw image files for analysis in IDEAS (version 6.2). For the dose response calibration curve,

peripheral blood was collected with informed consent (approved by Health Canada's Research Ethics Board) from healthy, non-smoking anonymous donors (three male and three female between the ages of 27 and 48). For the blinded samples, nine blood samples were collected from five healthy anonymous donors (males between the ages of 34 and 56 years of age) in 6 mL lithium-heparinized Vacutainer® tubes (BD Biosciences, Mississauga, ON) with the same health and historical radiation exposure criteria as described above. Each whole blood sample was then irradiated to a known dose between 0 and 4 Gy and blinded before culture. The doses were 0, 0.5, 0.7, 1.3, 1.7, 2.4, 2.9, 3.1, and 3.9 Gy. The CBMN assay was performed on all samples according to the procedure described in Rodrigues et al. (17–19). Briefly, whole blood samples were diluted with RPMI 1640 culture medium containing 10% fetal bovine serum, 2 mmol L-glutamine, 100 U/mL penicillin, 100 µg/mL streptomycin (Sigma–Aldrich, Oakville, ON) and 1% PHA (Life Technologies, Burlington, ON) to achieve 20 mL cultures in 25 cm<sup>2</sup> vented flasks. The cultures were incubated for 24 h before the addition of cytochalasin B (Sigma–Aldrich) then incubated for an additional 48 h. Cell suspensions were centrifuged, resuspended in FACS Lysing Solution (BD Biosciences) to lyse red blood cells and fix lymphocytes, washed twice with PBS and resuspended in 100 µL of PBS. All samples in solution were stained with a 1:100 dilution of DRAQ5 (eBioscience, San Diego, CA) to a final concentration of 1.25 nM per 1×10<sup>7</sup> cells/mL and run on the IS<sup>X</sup> at 40× magnification with the 658 nm laser set to 20 mW to allow DRAQ5 signal to be collected in channel 5 and the BF LED in channel 1 (18). Early in the development of this method we examined the extended depth of field (EDF) option on the IS<sup>X</sup> and found no improvement in image quality and therefore, all data were collected without the EDF. For the calibration curve, approximately 100,000 events were collected in about 20 min at each dose point for each donor. For the blinded samples, events were collected for 40 min in 5 min increments. For all acquisitions, a minimum area threshold was set to 75 pixels (18.75 µm<sup>2</sup>) in both channels 1 and 5 resulting in a collection speed of approximately 100–150 events per second which was related directly to the cell concentrations of 1–2 × 10<sup>7</sup> cells/mL. An event is defined as any image collected by the IS<sup>X</sup> that meets both criteria and is stored in the data file.

## RESULTS

### BNC and MN Mask Development and Gating Strategy in IDEAS

In IDEAS, a mask identifies pixels within a defined region of in an image. Optimized BNC and MN masks were developed by applying and combining several new and existing mask functions in IDEAS (version 6.2). The steps to create both masks are outlined below.

The BNC mask was optimized to better delineate pixels in the main nuclei to allow more precise classification of BNCs based on the intensity, shape, and size of individual nuclei. This was achieved by applying three sequential mask

functions as shown in Figure 1A. The first row shows the BF image and the second row shows the unmasked DRAQ5-stained nuclei. The third row shows the default event mask (superimposed blue on the main nuclei and MN) which is designed to highlight all pixels above background in an image. To create a BNC-specific mask, the Levelset function (fourth row) was first used to create a tight mask around the two main nuclei (intensity setting: medium, contour detail scale: 3). Next, the Watershed function was applied to the Levelset mask which allowed for separation of the two main nuclei by creating a border for the intensity valley within the nuclear image (fifth row). The Range function was then applied to the Watershed (Levelset) mask to exclude spots smaller than the main nuclei by setting a minimum area threshold of 115 pixels (28.7 µm<sup>2</sup>) resulting in the final BNC mask that excludes the MN in both images (sixth row). In order to quantify features of individual nuclei within the BNC mask, the Component mask was applied to identify individual nuclei using Area as the ranking feature (seventh and eighth rows).

The new MN mask, created using a combination of the Spot, Dilate and Morphology functions, identifies DRAQ5 stained spots that are separate from the main nuclei. This more specific MN mask allowed the minimum area to be reduced from 10 pixels (2.5 µm<sup>2</sup>) to 6 pixels (1.5 µm<sup>2</sup>), thereby allowing the scoring of smaller MN as compared to the previous analysis. Figure 1B demonstrates the process for two BNCs containing MN with the first row illustrating the cytoplasm visualized in the BF channel. The first spot identification function (second row) highlights spots in the image with radii between 1 and 4 pixels and a spot-to-cell background value of 2 and the Levelset function mask (third row), dilated by two pixels, identifies the main nuclei. Subtracting the dilated Levelset function mask from the first spot identification mask gives the first MN spot mask (fourth row) and ensures that no spots highlighted in the main nuclei are identified as MN. The second spot identification function (fifth row) highlights spots in the image with radii between 1 and 4 pixels and a spot-to-cell background value of 1 and the morphology function mask dilated by three pixels (sixth row), is used to highlight the main nuclei. Subtracting the morphology function mask from the second spot identification mask gives the second MN spot mask (seventh row) and allows for smaller nuclei (1.5 µm<sup>2</sup>) to be masked than can be achieved by the first MN spot mask while ensuring that no small artifacts near the edge of the main nuclei are incorrectly masked as MN. The final spot mask (eighth row) is a combination of the two spot masks and ensures that MN identified by either mask are correctly scored.

Figure 2 shows images captured by the IS<sup>X</sup> that highlight the improvements in the optimized BNC and MN masks over the original masks. The optimized BNC mask more tightly highlights the main nuclei in comparison to the original BNC mask (Fig. 2A). Small and large MN residing close to the main nuclei that were previously enveloped by the original BNC mask are no longer enveloped by the optimized BNC mask and are now correctly scored by the optimized MN

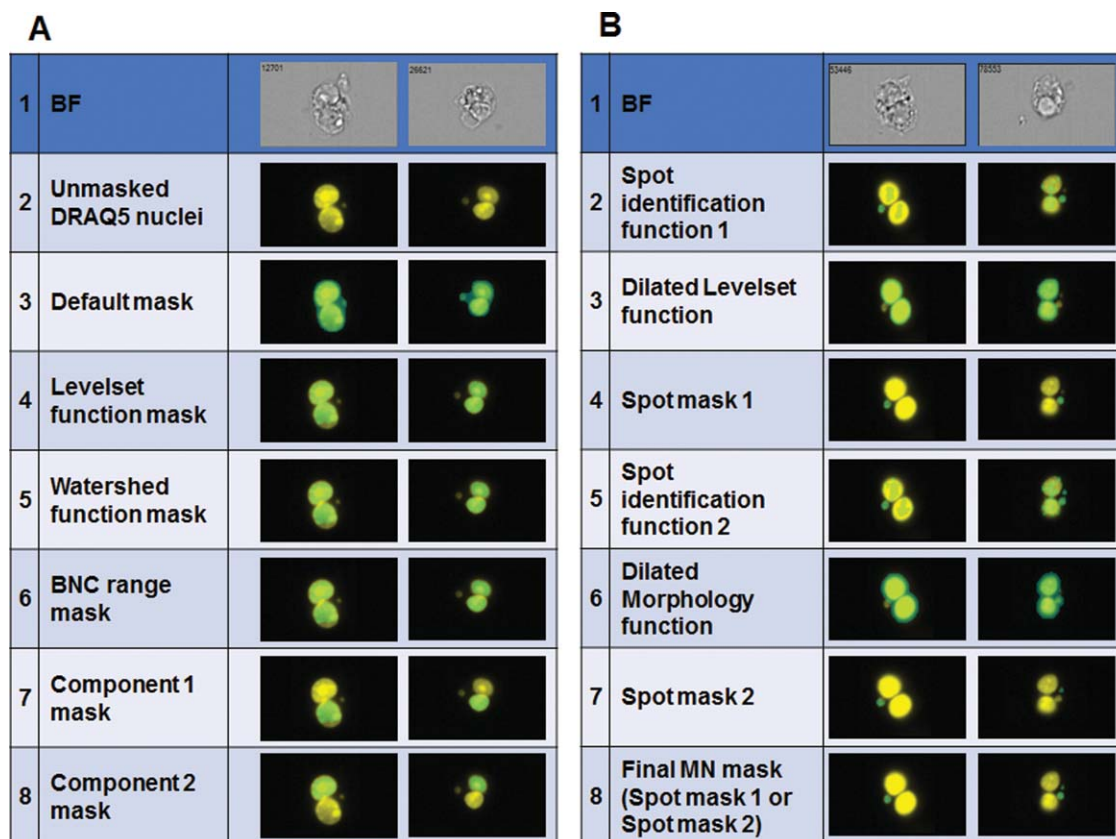


**Figure 1.** (A) The various steps used to create the optimized BNC mask illustrating improvement over the default mask (third row) through sequential combination of the Levelset (fourth row), Watershed (fifth row) and Range functions. The final BNC mask (sixth row) as well as the new component masks to highlight individual main nuclei (seventh and eighth rows) are shown. (B) The steps used to create the optimized MN mask. The spot identification function (second row) and dilated Levelset function (third row) are used to create the first spot mask (fourth row) while the spot identification function (fifth row) and the dilated morphology function (sixth row) are used to create the second spot mask (seventh row). Both spot masks are combined such that MN masked by either function are scored (eighth row).

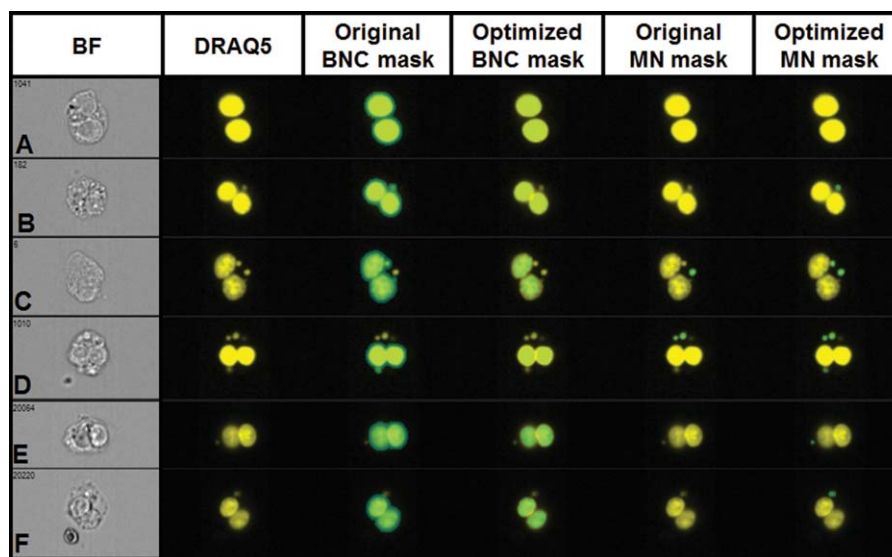


**Figure 2.** Various cell images illustrating the improvement of the optimized BNC and MN masks over the original masks. (A) A BNC with zero MN. (B) A BNC with one MN that was enveloped by the original BNC mask. (C, D) BNCs with two and three MN, respectively, showing that the original BNC mask enveloped one of the MN. (E, F) BNCs with MN that were unmasked by the original MN mask now being correctly identified by the optimized MN mask.

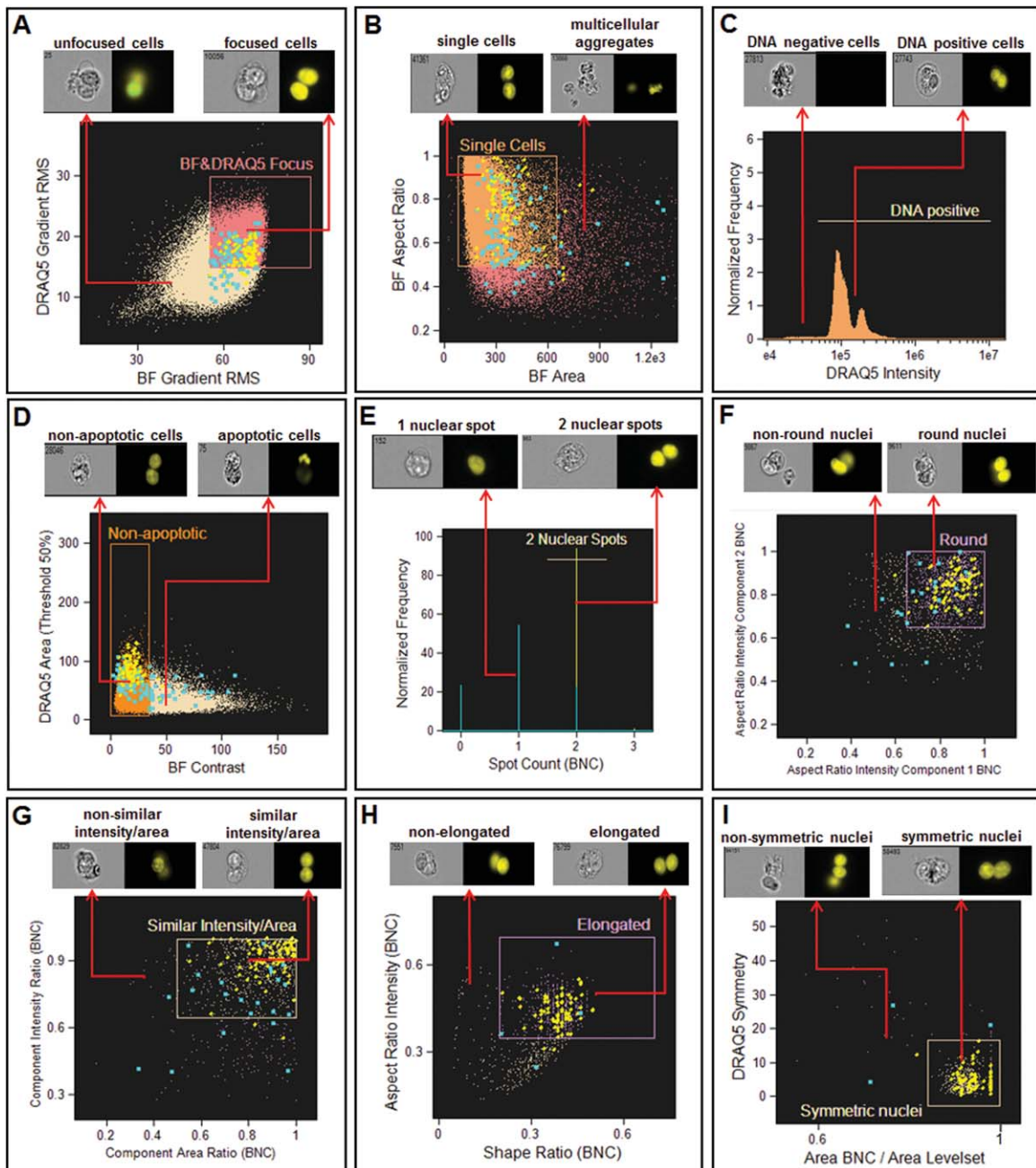


**Figure 3.** (A) Bivariate plot of *DRAQ5 Gradient RMS* versus *BF Gradient RMS* for the selection of focused cells. (B) Bivariate plot of *BF ASPECT RATIO* versus *BF AREA* for elimination of small debris and multicellular aggregates. (C) Histogram of *DRAQ5 INTENSITY* used to eliminate events with insufficient nuclear stain. (D) Bivariate plot of *DRAQ5 AREA* versus *BF CONTRAST* for elimination of apoptotic cells. (E) A *SPOT COUNT* histogram following application of the BNC mask which separated cells containing two separate masked nuclear spots from all other events. (F) Bivariate plot of *ASPECT RATIO INTENSITY* components allowing for circularity comparison of the two main nuclei. (G) Bivariate plot of *COMPONENT INTENSITY RATIO* versus *COMPONENT AREA RATIO* allowing for selection of events which contained two main nuclei that were similar in both area and intensity. (H) Bivariate plot of *ASPECT RATIO INTENSITY* versus *SHAPE RATIO* that allowed for removal of events that contained two distinct but overlapping nuclei. (I) Bivariate plot of *DRAQ5 SYMMETRY* versus the ratio of *BNC AREA to Levelset AREA* for selection of cells with two well-separated, distinct nuclei. The tagged BNC and non-BNC populations are represented by the yellow squares/bins and blue squares/bins, respectively. Representative images captured by the IS<sup>X</sup> are shown in each panel.

mask (Figs. 2B–2D). In addition, smaller MN and MN that were previously missed by the limitations of the original MN mask are now correctly scored by the optimized MN mask (Figs. 2E and 2F).

### Gating Strategy in IDEAS

To filter, identify and score BNCs and MN, an optimized analysis template using new features and image masks developed by Amnis<sup>®</sup> was created in IDEAS. To

**Table 1.** Summary of all features used to develop the IDEAS<sup>®</sup> analysis template described in Figure 3. The feature and purpose for its use as well as the gate boundaries used in each panel in Figure 3 are shown

| FIGURE PANEL | FEATURES                           | GATE BOUNDARIES (MIN/MAX) | PURPOSE OF FEATURE  |
|--------------|------------------------------------|---------------------------|---|
| 3A           | DRAQ5 GRADIENT RMS                 | 15/NA                     | Selects for single, non-apoptotic, DNA-positive cells   |
|              | BF GRADIENT RMS                    | 55/NA                     |   |
| 3B           | BF ASPECT RATIO                    | 0.5/1                     | Eliminates coincident doublet events, retains the majority of BNCs  |
|              | BF AREA                            | 85/650                    | Eliminates small debris and multicellular aggregates  |
| 3C           | DRAQ5 INTENSITY                    | $1 \times 10^5$ /NA       | Removes events with insufficient nuclear content to be a BNC  |
| 3D           | DRAQ5 AREA                         | 10/300                    | Removes apoptotic events  |
|              | BF CONTRAST                        | 0/35                      |   |
| 3E           | SPOT COUNT                         | 1.5/2.5                   | Removes all events that do not have two distinct nuclei   |
| 3F           | ASPECT RATIO INTENSITY COMPONENT 1 | 0.65/1                    | Compares the circularity of each of the main nuclei in each BNC against one another <sup>a</sup>  |
|              | ASPECT RATIO INTENSITY COMPONENT 2 | 0.65/1                    |   |
| 3G           | COMPONENT INTENSITY RATIO (BNC)    | 0.65/1                    | Selects for BNCs having two nuclei with similar DRAQ5 intensity <sup>a</sup>  |
|              | COMPONENT AREA RATIO (BNC)         | 0.5/1                     | Selects for BNCs having two nuclei with similar area  |
| 3H           | ASPECT RATIO INTENSITY             | 0.35/0.7                  | Selects for events that contain two distinct, non-overlapping nuclei <sup>a</sup>   |
|              | SHAPE RATIO                        | 0.2/0.7                   |   |
| 3I           | DRAQ5 SYMMETRY                     | 0/15                      | Differentiates between objects that have two-fold versus three-fold axes of symmetry. Objects within the gate boundaries have only two DRAQ5 stained nuclei |
|              | AREA BNC/AREA Levelset             | 0.8/1                     |   |

<sup>a</sup>Based on scoring criteria developed by Fenech et al. (9).

quantitate the gating process, separate populations containing 100 BNCs and 100 non-BNCs were selected at each dose point for one donor by manually highlighting (tagging) images from the original unfiltered population without visualizing the analysis area in IDEAS. This ensured unbiased selection of images. BNCs and non-BNCs were tagged according to the traditional scoring criteria described by Fenech et al. (9). These events (BNCs, yellow; non-BNCs, blue) were then identified on each panel in Figure 3 such that they could be tracked sequentially through the template. This allowed gate dimensions to be optimized such that no more than 10% of the BNC population was gated out in any plot and as many as possible non-BNC events were gated out. Details of the features, functions, masks and gating strategies used to optimize the data analysis template are summarized in Table 1. To automatically count the frequency of MN within the final BNC population, the *SPOT COUNT* feature was applied to the newly developed MN mask and a histogram of MN frequency was generated

(Fig. 4), similar to the histograms generated in our previous work (17,18). Representative images are also shown to demonstrate typical events found in each bin.

### Dose Response Calibration Curves and Blinded Samples

Six independent experiments with six different donors were carried out in a previous study to generate a dose response calibration curve (18). In the current study, the data files from that work were re-analyzed with the optimized IDEAS template described above to demonstrate improvement in detection and scoring of BNCs and MN.

One-hundred BNC and one-hundred non-BNC events were tagged in data files across the 0–4 Gy dose range for one donor in order to illustrate the efficiency with which each gate filtered these populations by incorporating the BNC scoring criteria described by Fenech et al. (9). Their distribution is demonstrated in Figure 3 and Table 2 provides supporting statistics across the dose range for both the original and optimized gating

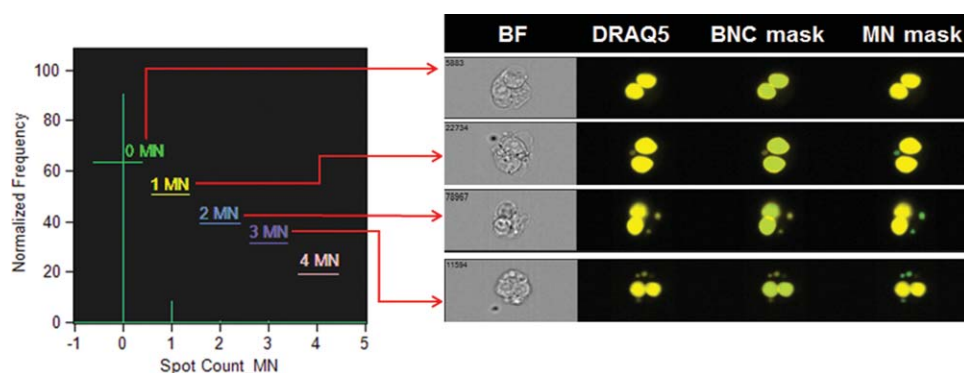


**Figure 4.** Histogram of the *SPOT COUNT* applied to the MN mask using final BNC population from a sample irradiated with 2 Gy. Representative images captured by the IS<sup>X</sup> are shown in each panel.

and masking strategies. The optimized IDEAS analysis template demonstrates an improvement across the dose range in BNC detection accuracy, recovering 25% of the tagged BNCs eliminated with the original template, and eliminating 83% of tagged non-BNCs retained with the original template. On average, 849 BNCs were scored across the 0–4 Gy dose range for each donor at each data point (Table 2), a reduction of a factor of about three as compared to the 2647 BNCs identified by the original BNC mask on average across the dose range. This reduction demonstrates that the gating strategy more effectively filters unwanted events and that the optimized BNC mask is more selective of true BNCs within the final population. Furthermore, Table 2 demonstrates that the optimized MN mask identified more MN (an average of 99 MN across the dose range) than the original MN mask (an average of 87 MN across the dose range) despite the fact that fewer BNCs were identified,

illustrating an increase in sensitivity of the optimized MN mask.

Figure 5A presents the rate of MN per BNC as a function of dose for all six donors, the average rate of MN per BNC at the 95% confidence intervals as determined in Matlab (version 7.11.0.584, Mathworks, MA). A quadratic increase with dose up to 4 Gy is expected from biological considerations (3), historical work on the CBMN assay (4,5,23) and from our previous work with IS<sup>X</sup>-CBMN method (17–19) and was observed in this work. At 0 Gy, the average rate of MN per BNC at 0 Gy for all six donors was 0.022 which was within the 0–0.040 range typical of background MN frequencies (24). Variability in the rate of MN per BNC with increasing dose, which was observed in our previous work (17–19), was once again observed here as the rate of MN per BNC varied between approximately 0.30–0.45 for all donors at 4 Gy.

**Table 2.** The percentage of 100 tagged BNCs and non-BNCs remaining following application of each gate in the optimized IDEAS<sup>®</sup> analysis template at each dose point for one donor. The percentage of events remaining in the final BNC population in the original analysis template is also shown (18). The numbers of BNCs and MN scored are also shown for one donor across the dose range from both the optimized and original analysis templates

| GATE                                       | % BNCs REMAINING |       |       |       |       |       | % NON-BNCs REMAINING |      |      |      |      |      |
|--|------------------|-------|-------|-------|-------|-------|----------------------|------|------|------|------|------|
|  | 0 Gy             | 1 Gy  | 2 Gy  | 3 Gy  | 4 Gy  | AVG.  | 0 Gy                 | 1 Gy | 2 Gy | 3 Gy | 4 Gy | AVG. |
| BF & DRAQ5 Focus                           | 86               | 92    | 96    | 91    | 89    | 91    | 27                   | 56   | 64   | 75   | 80   | 60   |
| Single cells                               | 86               | 88    | 96    | 84    | 89    | 89    | 24                   | 50   | 30   | 59   | 64   | 45   |
| DRAQ5 positive                             | 86               | 88    | 96    | 84    | 89    | 89    | 24                   | 49   | 30   | 59   | 64   | 45   |
| Non-apoptotic                              | 84               | 88    | 96    | 81    | 89    | 88    | 17                   | 34   | 12   | 30   | 44   | 27   |
| Two nuclear spots                          | 83               | 84    | 88    | 81    | 86    | 84    | 10                   | 0    | 8    | 6    | 14   | 8    |
| Round                                      | 81               | 83    | 87    | 80    | 85    | 83    | 9                    | 0    | 6    | 6    | 9    | 6    |
| Similar intensity/area                     | 81               | 83    | 85    | 78    | 83    | 82    | 8                    | 0    | 5    | 4    | 6    | 5    |
| Elongated                                  | 78               | 79    | 84    | 76    | 82    | 80    | 3                    | 0    | 3    | 3    | 3    | 2    |
| Symmetric nuclei<br>(final BNC population) | 78               | 79    | 82    | 75    | 80    | 79    | 0                    | 0    | 3    | 0    | 1    | 1    |
| Original template<br>(final population)    | 76               | 86    | 79    | 61    | 59    | 72    | 14                   | 3    | 1    | 5    | 6    | 6    |
|  | BNCs SCORED      |       |       |       |       |       | MN SCORED            |      |      |      |      |      |
|  | 0 Gy             | 1 Gy  | 2 Gy  | 3 Gy  | 4 Gy  | AVG.  | 0 Gy                 | 1 Gy | 2 Gy | 3 Gy | 4 Gy | AVG. |
| Optimized template                         | 1,088            | 1,016 | 692   | 721   | 728   | 849   | 21                   | 49   | 78   | 147  | 203  | 99   |
| Original template                          | 2,169            | 2,939 | 2,497 | 2,864 | 2,766 | 2,647 | 20                   | 42   | 70   | 127  | 174  | 87   |

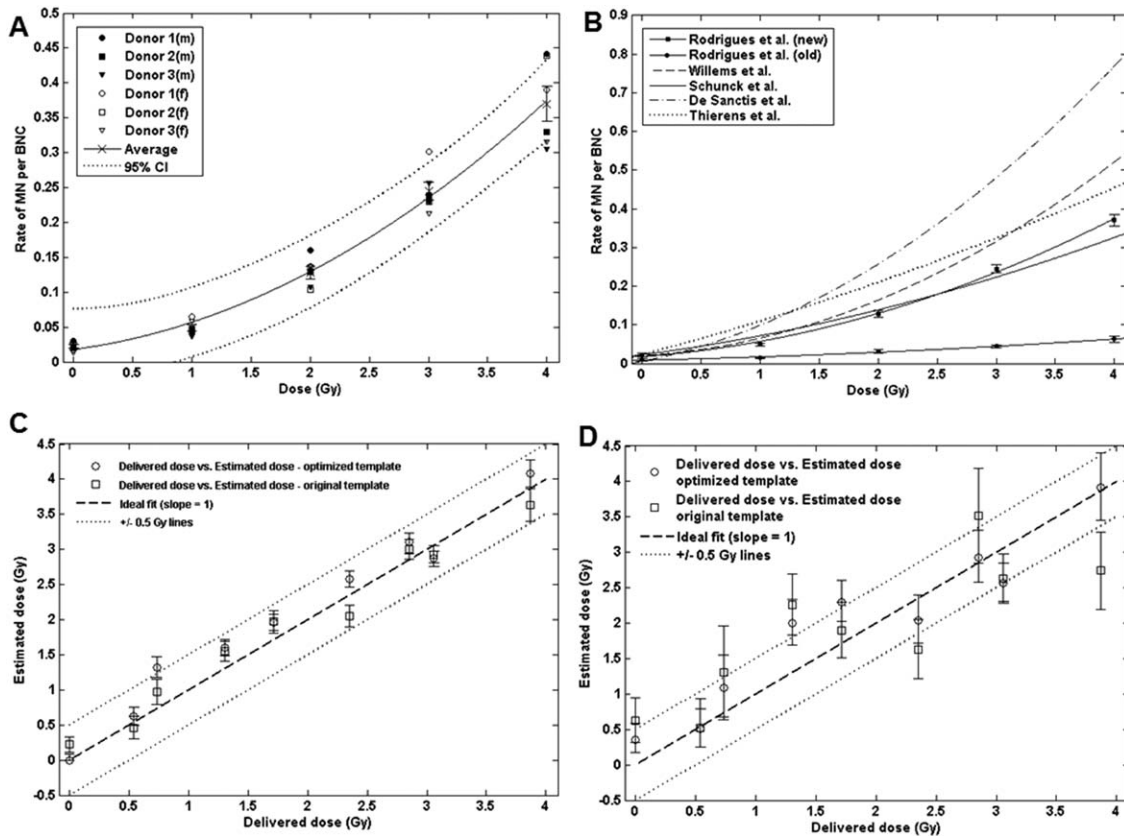


**Figure 5.** (A) The rate of MN per BNC versus dose for six donors (three male, three female). The average rate of MN per BNC at each dose point is also plotted, the error bars represent the standard error of the mean and the dashed lines represent the 95% confidence intervals. (B) The average rate of MN per BNC from A (squares) and the average rate of MN per BNC from our previous work in Rodrigues et al. (18) (circles) including error bars which represent the standard error of the mean. The rate of MN per BNC from Schunck et al. (7) (solid line), Willems et al. (25) (dashed line), De Sanctis et al. (26) (dashed-dotted line), and Thierens et al. (27) (dotted line) are also plotted using the equations provided in those publications. (C, D) Estimated dose (Gy) versus delivered dose (Gy) determined by the IS<sup>X</sup>-CBMN method for nine blinded samples using the optimized (circles) and original (squares) IDEAS<sup>®</sup> analysis templates following 40 min (C) and 5 min (D) of data collection. The dashed line represents a slope of one, where the estimated dose would equal the delivered dose and the dotted lines represent  $\pm 0.5$  Gy from the ideal slope. The error bars represent the standard error on the estimated dose.

However, the deviation from the average rate of MN per BNC was calculated to be only 15% on average for all donors across the dose range, compared to 26% in our previous work (18). The average rate of MN per BNC ( $Y$ ) as a function of dose ( $D$ ) was fitted to the following quadratic equation in Matlab:

$$Y = 0.0185 + 0.0237D + 0.0106D^2. \quad (1)$$

Figure 5B shows the average calibration curve for the rate of MN per BNC from both Figure 5A and our previous work (18). Also plotted in Figure 5B are calibration curves from Schunck et al. (7), Willems et al. (25), De Sanctis et al. (26), and Thierens et al. (27). These curves were plotted using the quadratic equations provided by the authors and demonstrate the variability between calibration curves using automated slide-scoring based versions of the CBMN assay. In addition, Figure 5B demonstrates that the rate of MN per BNC has increased by a factor of about six at the 4 Gy dose, illustrating the effectiveness and accuracy of both the optimized BNC and MN masks.

Figures 5C and 5D show graphical representations of the delivered dose (Gy) versus the estimated dose (Gy) (black

circles) for all nine blinded samples after collecting data on the IS<sup>X</sup> for 40 and 5 min, respectively. Also plotted are the dose estimations from our previous work (19) (black squares), the ideal line with a slope of 1 where the delivered dose and the estimated dose would be equal (dashed line) as well as the  $\pm 0.5$  Gy lines (dotted lines). All dose estimations were determined using CABAS v2 (Chromosome Aberration Calculation Software) (28) and the error bars represent the standard errors (SE) on the dose estimations. Figure 5C illustrates that after 40 min of data collection, the newly optimized analysis template was able to estimate blinded doses to within 0.5 Gy of the delivered dose in all but the 0.73 Gy sample (0.59 Gy higher than the delivered dose). The error bars associated with each data point are also within the  $\pm 0.5$  Gy lines in all but the 0.73 Gy sample. On average, 1,873 BNCs were scored for each sample after 40 minutes of data collection.

Figure 5D illustrates that after only 5 min of data collection, optimized analysis template was able to correctly estimate more blinded samples to within 0.5 Gy of the delivered dose than was possible with the original analysis template. Seven of the nine blinded samples were estimated correctly to

within 0.5 Gy as compared to only three of the nine samples with the original analysis template. On average, 280 BNCs were scored for each sample after only 5 minutes of data collection.

## DISCUSSION

In several recent publications, we have introduced a newly developed method for performing the CBMN assay using imaging FCM as a dose estimation tool in radiation biodosimetry (17–19). In the present study, we developed a new analysis strategy using mask functions recently implemented in IDEAS, and evaluated the performance of this analysis compared to our previous approach. First, hand-tagged truth populations (BNC and non-BNC, MN, and non-MN events) were selected which allowed for the identification of features that were able to distinguish between these populations. Direct visualization of the locations of these populations (Fig. 3) also allowed for ranges of all features to be optimized. Second, we discovered that an analysis template optimized for a single data file was, in many cases, not ideal for all conditions. By merging data collected from multiple donors at multiple dose points, the most optimized analysis template for all data files was achieved. Finally, data collected from blinded samples was used to confirm the accuracy of the optimized analysis. These strategies enabled us to substantially increase the comparability of this assay to previous published results in the literature and improve accuracy when generating dose estimations compared to our previous work.

Figure 3 shows the sequential application of bivariate plots and histograms in the analysis template and demonstrates the effectiveness with which BNCs could be separated from cellular debris and other undesired objects in the data acquired by the IS<sup>X</sup>. While identification of focused, single cells can be attained from the BF images, the addition of a DRAQ5 nuclear stain also allows apoptotic cells to be gated out based on the hallmarks of apoptosis (chromatin condensation, nuclear condensation, and increased blebbing) without the use of an additional viability dye (13). All DRAQ5 stained BNCs were shown to fall between  $1 \times 10^5$  AU and  $1 \times 10^6$  AU of intensity indicating that the main nuclei show a relatively uniform uptake of DRAQ5. This result may allow for improved data collection to be obtained through the application of more stringent intensity classifiers on the IS<sup>X</sup> which would filter out more unwanted events during acquisition. Furthermore, the newly created BNC mask was able to better differentiate images with two DRAQ5 stained objects from those with zero, one or three or more DRAQ5 stained objects compared to the previous versions of the IDEAS template. Several of the new features developed in IDEAS that simultaneously compare the main nuclei to one another based on circularity, size, staining intensity and symmetry, allowed BNCs to be further differentiated from other undesired events. By implementing these cell-specific parameters in the IDEAS template, 99% of the tagged non-BNCs were correctly filtered from the final population on average across the dose range. In addition, 25% of the tagged BNCs eliminated with the origi-

nal template were recovered and 83% of the tagged non-BNCs retained with the original template were eliminated.

Figure 5 demonstrates that the optimized IDEAS analysis template generates a dose response calibration curve that is of similar magnitude to those presented in the literature and that the dose estimations from blinded samples generated using this curve are more accurate. The rate of MN per BNC as a function of dose demonstrates some variability between donors. This variability in the CBMN assay has been well documented in the literature and Kacprzak et al. (29) showed that for five donors, the rate of MN per 1,000 BNC was relatively consistent at 0 Gy but had an approximate range of 0.2–0.6 at 5 Gy. While the variability between donors across the dose range has been reduced in this work to 15% compared to 26% in our previous analysis template (18), the need for generating a calibration curve that is based on the rate of MN per BNC from multiple donors is demonstrated. In addition, the magnitude of the rate of MN per BNC in this work has increased by a factor of about four in comparison to our previous work, on average, across the dose range, illustrating the effectiveness of the optimized BNC and MN masks. In previous versions of the IDEAS analysis template, MN close to the main nuclei and smaller MN could not be scored due to the limitations in the available masking parameters, however the optimized MN mask is now able to correctly score these events which has led to the observed improvement.

In order to determine if the improvement in BNC and MN identification corresponded to an increase in accuracy when generating dose estimations, data acquired from nine samples previously irradiated and blinded (19) were re-analyzed. Figure 5C demonstrates that the optimized IDEAS analysis template was able to correctly estimate eight of the nine doses to within 0.5 Gy after 40 min of data collection, with only the 0.73 Gy sample falling outside the  $\pm 0.5$  Gy limits. Figure 5D illustrates the improved accuracy of the optimized analysis template and demonstrates that dose estimations for seven of the nine doses were correct to within 0.5 Gy after only 5 min of data collection. This is a significant improvement over the original analysis template which was only able to correctly estimate three of the nine doses to within 0.5 Gy following 5 min of data collection. On average, 280 BNCs were scored for each blinded sample after only 5 min of data collection, but in some cases, <200 BNCs were scored. McNamee et al. have previously recommended that 200 BNCs be scored to provide reliable dose estimations (23). Furthermore, in a recent publication De Amicis et al. were able to successfully identify doses up to 4 Gy, within 0.5 Gy of the delivered dose by scoring only 100 BNCs (30). The results of this work are consistent with the results of De Amicis et al. and demonstrate that scoring approximately 100 BNCs was sufficient to produce accurate dose estimations between 0 and 4 Gy. Overall, this demonstrates that the new IDEAS analysis template is able to provide dose estimations with acceptable accuracy (within  $\pm 0.5$  Gy) after only 5 min of data collection and in some cases, after scoring only 100 BNCs.

This paper has introduced the application of new features and masks developed in the IDEAS software designed specifically for improved detection of BNCs and MN in the IS<sup>X</sup>-based version of the CBMN assay with applications in radiation biodosimetry. Using these tools, an optimized data analysis template was created which more effectively identified BNCs and quadrupled the frequency of scored MN across the 0–4 Gy dose range. This new analysis method allowed for the generation of a dose response calibration curve that was similar in magnitude to those presented in the literature which were generated by automated slide scoring methods. Finally, dose estimations of blinded samples were correctly generated to within 0.5 Gy of the delivered dose following only 5 minutes of data collection on the IS<sup>X</sup>, a marked improvement over our previous work. The improved analysis template, combined with the reduction in data collection time on the IS<sup>X</sup>, will allow for increased accuracy and throughput when performing biodosimetry to estimate unknown radiation doses received by exposed individuals following large-scale radiological or nuclear emergencies.

#### LITERATURE CITED

- Alexander GA, et al. BidosEPR-2006 meeting: Acute dosimetry consensus committee recommendations on biodosimetry applications in events involving uses of radiation by terrorists and radiation accidents. *Radiat Meas* 2007;42:972–996.
- Rea ME, Gougelet RM, Nicolalde RJ, Geiling JA, Swartz HM. Proposed triage categories for large-scale radiation incidents using high-accuracy biodosimetry methods. *Health Phys* 2010;98:136–144.
- Hall EJ, Giaccia AJ. *Radiobiology for the Radiologist*. Philadelphia, PA: Lippincott Williams & Wilkins; 2012.
- Fenech M, Morley AA. Measurement of micronuclei in lymphocytes. *Mutat Res* 1985;147:29–36.
- Fenech M, Morley AA. Cytokinesis-block micronucleus method in human lymphocytes—Effect of in vivo aging and low dose x-irradiation. *Mutat Res* 1986;161:193–198.
- Sullivan JM, Prasanna PGS, Grace MB, Wathen LK, Wallace RL, Koerner JF, Coleman CN. Assessment of biodosimetry methods for a mass-casualty radiological incident: Medical response and management considerations. *Health Phys* 2013;105:540–54.
- Schunck C, Johannes T, Varga D, Lorch T, Plesch A. New developments in automated cytogenetic imaging: Unattended scoring of dicentric chromosomes, micronuclei, single cell gel electrophoresis, and fluorescence signals. *Cytogenet Genome Res* 2004;104:383–389.
- Varga D, Johannes T, Jainta S, Schuster S, Schwarz-Boeger U, Kiechle M, Garcia BP, Vogel W. An automated scoring procedure for the micronucleus test by image analysis. *Mutagenesis* 2004;19:391–397.
- Fenech M, Chang WP, Kirsch-Volders M, Holland N, Bonassi S, Zeiger E. HUMN project: Detailed description of the scoring criteria for the cytokinesis-block micronucleus assay using isolated human lymphocyte cultures. *Mut Res - Genet Toxicol Environ Mut* 2003;534:65–75.
- Tamizh Selvan G, Chaudhury NK, Venkatachalam P. Comparison of results of the manual and automated scoring of micronucleus frequencies in 60Co-irradiated peripheral blood lymphocytes for triage dosimetry. *Appl Radiat Isot* 2015;97:70–77.
- Avlasevich SL, Bryce SM, Cairns SE, Dertinger SD. In vitro micronucleus scoring by flow cytometry: Differential staining of micronuclei versus apoptotic and necrotic chromatin enhances assay reliability. *Environ Mol Mut* 2006;47:56–66.
- Bryce SM, et al. Interlaboratory evaluation of a flow cytometric, high content in vitro micronucleus assay. *Mut Res Genet Toxicol Environ Mut* 2008;650:181–195.
- Bryce SM, Avlasevich SL, Bemis JC, Phonethpawth S, Dertinger SD. Miniaturized flow cytometric in vitro micronucleus assay represents an efficient tool for comprehensively characterizing genotoxicity dose–response relationships. *Mut Res Genet Toxicol Environ Mut* 2010;703:191–199.
- Bryce SM, et al. Flow cytometric 96-well microplate-based in vitro micronucleus assay with human TK6 cells: Protocol optimization and transferability assessment. *Environ Mol Mut* 2013;54:180–194.
- Bryce SM, Bemis JC, Avlasevich SL, Dertinger SD. In vitro micronucleus assay scored by flow cytometry provides a comprehensive evaluation of cytogenetic damage and cytotoxicity. *Mut Res Genet Toxicol Environ Mut* 2007;630:78–91.
- Fenech M. The lymphocyte cytokinesis-block micronucleus cyto assay and its application in radiation biodosimetry. *Health Phys* 2010;98:234–243.
- Rodrigues MA, Beaton-Green LA, Kutzner BC, Wilkins RC. Automated analysis of the cytokinesis-block micronucleus assay for radiation biodosimetry using imaging flow cytometry. *Radiat Environ Biophys* 2014a;53:273–282.
- Rodrigues MA, Beaton-Green LA, Kutzner BC, Wilkins RC. Multi-parameter dose estimations in radiation biodosimetry using the automated cytokinesis-block micronucleus assay with imaging flow cytometry. *Cytometry Part A* 2014b;85A:883–893.
- Rodrigues MA, Beaton-Green LA, Wilkins RC. Validation of the cytokinesis-block micronucleus assay using imaging flow cytometry for high throughput radiation biodosimetry. *Health Phys* 2015;110:29–36.
- Basiji DA, Ortyń WE, Liang L, Venkatachalam V, Morrissey P. Cellular image analysis and imaging by flow cytometry. *Clin Lab Med* 2007;27:653–670.
- Ortyń WE, Perry DJ, Venkatachalam V, Liang L, Hall BE, Frost K, Basiji DA. Extended depth of field imaging for high speed cell analysis. *Cytometry Part A* 2007;71A:215–231.
- Zuba-Surma EK, Kucia M, Abdel-Latif A, Lillard JW Jr, Ratajczak MZ. The Image-Stream system: A key step to a new era in imaging. *Folia Histochem Cytobiol* 2007;45:279–290.
- McNamee JP, Flegal FN, Greene HB, Marro L, Wilkins RC. Validation of the cytokinesis-block micronucleus (CBMN) assay for use as a triage biological dosimetry tool. *Radiat Prot Dosim* 2009;135:232–242.
- IAEA. *Cytogenetic Dosimetry: Applications in Preparedness for and Response to Radiation Emergencies*. Vienna, EPR-Biodose; 2011.
- Willems P, August L, Slabbert J, Romm H, Oestreicher U, Thierens H, Vral A. Automated micronucleus (MN) scoring for population triage in case of large scale radiation events. *Int J Radiat Biol* 2010;86:2–11.
- De Sanctis S, De Amicis A, Di Cristofaro S, Franchini V, Regalbutto E, Mammana G, Lista F. Cytokinesis-block micronucleus assay by manual and automated scoring: Calibration curves and dose prediction. *Health Phys* 2014;106:745–749.
- Thierens H, et al. Is a semi-automated approach indicated in the application of the automated micronucleus assay for triage purposes? *Radiat Prot Dosim* 2014;159:87–94.
- Deperas J, et al. CABAS: A freely available PC program for fitting calibration curves in chromosome aberration dosimetry. *Radiat Prot Dosim* 2007;124:115–123.
- Kacprzak J, Kuszewski T, Lankoff A, Müller WU, Wojcik A, Lisowska H. Individual variations in the micronucleus assay for biological dosimetry after high dose exposure. *Mutat Res Genet Toxicol Environ Mut* 2013;756:196–200.
- De Amicis A, De Sanctis S, Di Cristofaro S, Franchini V, Regalbutto E, Mammana G, Lista F. Dose estimation using dicentric chromosome assay and cytokinesis block micronucleus assay: Comparison between manual and automated scoring in triage mode. *Health Phys* 2014;106:787–797.